JACS
JOURNAL OF THE AMERICAN CHEMICAL SOCIETY
Communication
pubs.acs.org/JACS

Compression-Induced Deformation of Individual Metal–Organic Framework Microcrystals

Zhi Su,[†] Yu-Run Miao,[†] Shi-Min Mao,[‡] Guang-Hui Zhang,[§] Shen Dillon,[‡] Jeffrey T. Miller,[§] and Kenneth S. Suslick*,[†]

[†]Department of Chemistry and [‡]Department of Materials Science and Engineering, University of Illinois at Urbana—Champaign, Urbana, Illinois 61801, United States

[§]Chemical Sciences and Engineering Division, Argonne National Laboratory, Argonne, Illinois 60439, United States

Supporting Information

ABSTRACT: The deformation and mechanical behavior of individual zeolitic–imidazolate framework (ZIF-8) micro- and sub-microcrystals were observed under compression. Young's modulus and volume changes as a function of applied pressure were determined on individual single crystals, offering insights in the relationship among structure, morphology, and mechanical properties. Dramatic volume decreases and amorphization were detected during compression over a pressure range of 0–4 GPa for individual 1.2 μm ZIF-8 microcrystals, and the deformed microcrystals partially recovered after pressure release. The orientation and size effects on the mechanical behavior of ZIF-8 nano- and microcrystals were also investigated. The presence of solvates within the pores of the ZIF-8 has a dramatic effect on the mechanical properties of the single crystals. Methanol-solvated ZIF-8 microcrystals are much less deformable than the desolvated microcrystals and shatter completely at very low applied force.

Porous metal–organic frameworks (MOFs) show promise for a wide range of applications—gas storage and separation, catalysis, drug delivery, etc.[1] MOF properties can be tuned by the choice of bridging ligands and metal ion coordination sites,[2] giving enormous porosities with BET surface areas as high as 7000 m^2/g. For many applications, the mechanical properties of MOFs will prove critical to their efficacy.[3] For example, maintenance of porosity is essential during sorption/desorption cycles, which can generate substantial cyclic stresses and strains. However, only limited research on the mechanical properties of MOFs has been reported.[3b,4]

Zeolitic–imidazolate frameworks (ZIFs) are an emerging class of MOFs that feature extended three-dimensional structures composed of tetrahedral metal ions bridged by imidazolate units.[5] ZIF-8 [$Zn(2\text{-MeIm})_2$, 2-MeIm = 2-methylimidazolate] exhibits a sodalite topology and has been widely studied due to its robust chemical and thermal stabilities.[4] It crystallizes in the cubic $I\bar{4}3m$ space group with an ideal tetrahedral geometry at Zn^{2+} that contains 11.6 Å diameter cavities connected via 3.5 Å diameter apertures made from six-bridged imidazolate rings and via four-bridged imidazolate rings which are nearly close packed (Figure 1).

When porous solids are subjected to pressure or shock, three mechanical processes are involved: (1) compaction (squeezing out void space between crystals through deformation of crystals), (2) compression (reduction of the internal porosity of porous crystals with the partial collapse of free pore volume inside the structure), and (3) cataclysmic ductile collapse (further collapse of the pore structure, fracture of the compacted crystals, and amorphization of the resulting solid).[6]

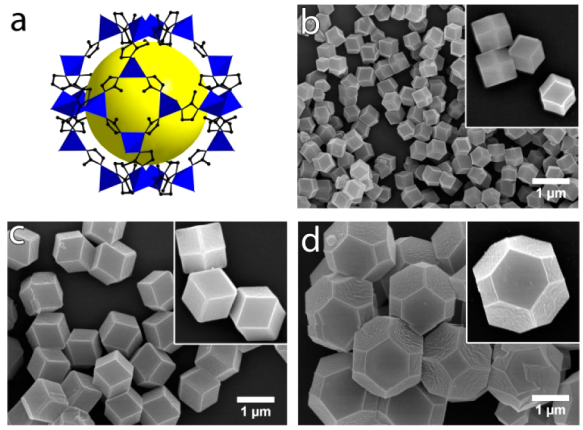

Figure 1. (a) Crystal structure of ZIF-8 with a truncated octahedral topology. Particle size and morphology were controlled by varying the concentration of the ligands and Zn(II) precursor. The molar ratio of 2-MeIm:1-MeIm:Zn^{2+} was maintained at 4:4:1. (b–d) SEM images of ZIF-8 crystals prepared with reaction concentrations of $Zn(NO_3)\cdot 6H_2O$ at (b) 0.125, (c) 0.05, and (d) 0.0125 mM. For (b) and (c), the morphology is rhombic dodecahedral; for (d) the morphology has changed to truncated rhombic dodecahedral. Insets are 2.5× magnified compared to the rest of the image.

We report here the use of *in situ* observation by transmission electron microscopy (TEM) during compression to directly visualize the deformation of individual ZIF-8 nano- and microcrystals. From these measurements, we are able to provide a quantitative load–displacement curve for individual crystals. TEM video recordings as a function of applied force provide a direct measure of dynamic deformation processes and the resulting load–displacement curve. Morphological changes of individual nano- and microcrystals observed under compression offer new insights into structure–morphology–mechanical relationships.

Received: November 4, 2014
Published: January 29, 2015

DOI: 10.1021/ja5113436
J. Am. Chem. Soc. 2015, 137, 1750–1753

ZIF-8 nano- and microcrystals were synthesized at room temperature to yield a narrow size distribution with well-defined morphologies (Supporting Information, Table S1).[7] Powder X-ray diffraction (PXRD) indicates that highly crystalline ZIF-8 crystals were obtained (Figure S1). The crystal size was controlled by the precursor concentrations. As shown in Figure 1, the crystals obtained could be size controlled (from 0.55 to 1.2 to 2.3 μm), with Zn(II) concentrations ranging from 0.125 to 0.05 to 0.0125 mM, respectively, while maintaining the molar ratio of each at 4:4:1 2-MeIm:1-MeIm:Zn^{2+}. The smaller crystals were rhombic dodecahedral, whereas the largest (2.3 μm) crystals were truncated rhombic dodecahedral (Figure S2). This morphology change must reflect differences in facet growth rates as a function of solution concentrations of the precursors.[8] All ZIF-8 crystals were desolvated at 250 °C for 5 h to remove guest solvates and placed in a desiccator until used.

For comparison with individual microcrystals, bulk samples (50 mg) of 1.2 μm desolvated ZIF-8 microcrystal pellets were prepared using a hydraulic piston pelletizer. The ZIF-8 microcrystals were packed in a 13 mm diameter die and vertically compressed to pressures as large as 1.9 GPa (25 ton load), which produced an irreversible morphological transition and amorphization upon the release of applied pressure. SEM shows that the ZIF-8 microcrystals underwent deformation at lower pressure, transforming from rhombic dodecahedra to irregular blocks (<0.8 GPa; Figure S3). As pressure was further increased, particle fracture followed, and the small, cracked fragments agglomerated by 1.9 GPa. Compression dramatically decreased the BET surface area from 1340 m^2/g for the initial solid to 253 m^2/g after treatment at 1.9 GPa, showing that the amorphous pressure-treated desolvated ZIF-8 microcrystals still remain partially porous (Table S2).

PXRD patterns of microcrystal samples pressurized up to 0.8 GPa show diffraction peaks that are consistent with maintaining the long-range order of the original sample, although the peak intensities are significantly decreased (Figure S4). In contrast, after pressurization >0.8 GPa and release, the XRD pattern loses most of the diffraction peaks, except one broadened weak peak at 6.6°, corresponding to a Zn−2-MeIm−Zn unit: amorphization is irreversible, and long-range order has been lost.

X-ray absorption spectroscopy (XAS)[9] was employed to examine the local structure around the Zn ions of ZIF-8 microcrystals before and after high pressure treatment. In the X-ray absorption near-edge spectra, the systematic intensity changes after application of increasing pressure suggests only minor changes in the local coordination geometry around Zn^{2+} (Figure S5). The Fourier-transformed extend X-ray absorption fine structure (EXAFS) spectra (Figure S6) show a continuous decrease of the intensity but no major changes in peak positions, confirming only minimal changes in local coordination geometry around Zn^{2+}.

For the *in situ* TEM compression test, an individual desolvated 1.2 μm ZIF-8 microcrystal with hexagonal projection on the (−101) facet was placed on a holder with a 1.3 μm flat face (Figures 2, S7, and S8). The height (i.e., the (010) oriented direction, which is the compression direction) and diameter (i.e., the (100) oriented direction, which is perpendicular to compression; Figures 2a and S9) were 835 nm and 1.05 μm, respectively. The punch (a flat square surface with a 3 μm edge length) compressed the crystal at 1 nm/s to achieve quasistatic compression. The morphological change was recorded by video TEM and correlated to the displacement (see Figures 2 and S10), starting from the rhombic dodecahedral crystal before compression to the final flattened pillar after recovery from compression. During compression, the height decreased as the diameter increased (Figure 2b−e) to a minimum size with a height and diameter of 225 nm and 1.35 μm, respectively (Figure 2e). After the pressure was completely released, the microcrystal slightly rebounded from its maximum compression to a height and diameter of 293 nm and 1.25 μm, respectively (Figure 2f), suggesting the ZIF-8 microcrystal has substantial plasticity despite its rigid sodalite structure.[10] In contrast to the bulk sample, no obvious cracking or fractures occurred during the compression test (Figure S10), indicating that microcrystal−microcrystal interactions are the dominant cause of cracking and fracturing.

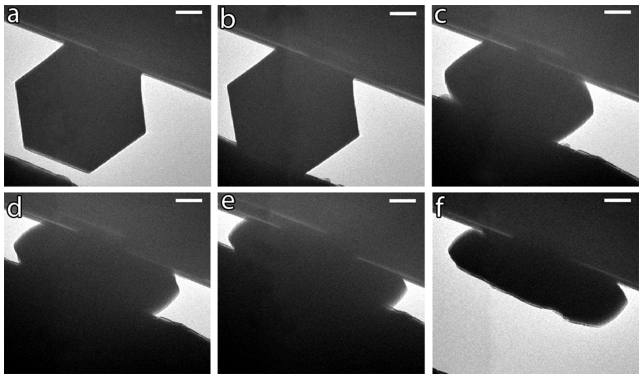

Figure 2. TEM images of a 1.2 μm ZIF-8 microcrystal (hexagonal projection) during the *in situ* compression test at various displacements: (a) before contact, at (b) 60, (c) 270, (d) 390, and (e) 480 nm displacement, and (f) after unloading. All scale bars are 200 nm.

The presence of solvates within the pores of the ZIF-8 has a dramatic effect on the mechanical properties of the single crystals. Methanol-solvated ZIF-8 microcrystals are much less deformable than the desolvated microcrystals and shatter completely at very low applied force (~600 μN at a displacement of 277 nm; Figures 3 and S11). Thus, the presence of solvate filling the pores of ZIF-8 makes the microcrystals extremely rigid with near total loss of plasticity, relative to desolvated crystals. Simulations suggest that the mechanical instabilities of ZIF-8 under compression are triggered by shear mode softening; we believe that such shear mode softening is likely repsonsible for the observed fracture of

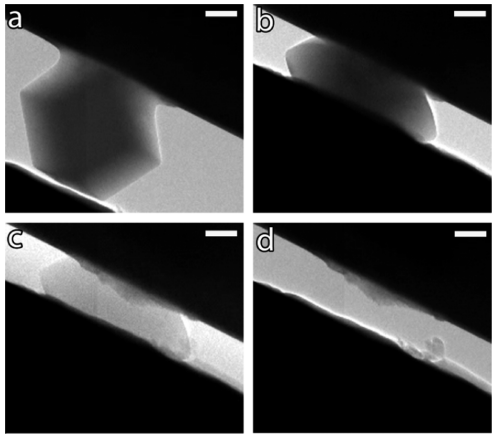

Figure 3. TEM images of a solvated 1.2 μm ZIF-8 microcrystal (hexagonal projection) during *in situ* compression at various displacements: (a) before contact and at (b) 276, (c) 277, and (d) 278 nm displacement, after complete fracture of crystal. All scale bars are 200 nm.

DOI: 10.1021/ja5113436
J. Am. Chem. Soc. 2015, 137, 1750−1753

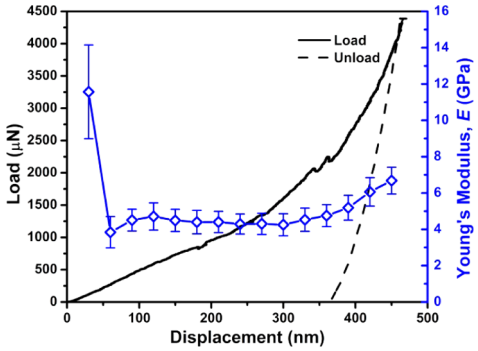

Figure 4. Left axis (black): Representative load−displacement curve of an *in situ* TEM compression test of a single 1.2 μm ZIF-8 microcrystal (hexagonal projection). The maximum load was ∼4300 μN. Solid and dashed lines are for the loading and unloading processes, respectively. Right axis (blue): Loading Young's modulus (E_{load}) as a function of displacement. Error bars are the standard deviation from ∼10 independent measurements.

solvated ZIF-8 crystals.[11] The simulations also examined the effect of methane loading within ZIF-8 and found that methane would delay amorphization compared to desolvated ZIF-8. We find the opposite, of course, with methanol as solvate, which may reflect the differences caused by the strong guest−ZIF-8 interactions between polar CH_3OH and the framework vs the absence of strong guest−ZIF-8 interaction with apolar CH_4. Young's (elastic) modulus (E) is a characteristic physical quantity of a material that measures the stiffness of that material. Young's Modulus during loading (E_{load}), which includes both plastic and elastic deformations, was calculated and plotted as a function of displacement (every 30 nm) for the ZIF-8 microcrystals. The unloading Young's modulus (E_{unload}), which includes only the elastic deformation, was calculated at the maximum force point (Figures 4 and S9).

A representative load−displacement curve of the 1.2 μm ZIF-8 microcrystal (hexagonal projection) is shown in Figure 4, where loading (compressing) is measured to a maximum force (∼4300 μN) and followed by complete unloading (0 μN). In Figure 4, E_{load} data from the first 100 nm of displacement must be disregarded due to the imperfect initial punch-to-sample surface contact. The loading modulus is fairly constant at 4.6 ± 0.2 GPa over a displacement range of 100−350 nm (equivalently, over a range of applied force of 500−2000 μN). Above a displacement of 350 nm, the modulus increases, suggesting that compression-induced amorphization is beginning to occur. The value for E_{unload} is much larger (41 ± 4 GPa) than the loading modulus as a consequence of the dense, amorphous phase of ZIF-8 microcrystals created under the maximum compression. This is the first time the mechanical behavior of an individual ZIF-8 microcrystal has been revealed.

The E_{load} value, 4.6 GPa, means ZIF-8 microcrystals have a stiffness similar to that of polystyrene (3−3.5 GPa) and much lower than those of pure metals (e.g., Al at 70 GPa, or Cu at 117 GPa). Our results are comparable to previous results from nanoindentation experiments on large single crystals (2.9−3.2 GPa)[12] and on micrometer-thick films (3.5 ± 0.2 GPa at 5% penetration) of ZIF-8 film.[13] In comparison, ZIF-8 microcrystals are tougher than MOF-5 (2.7 ± 1.0 GPa), reflecting the smaller cavity size and shorter bridging ligands for ZIF-8 vs MOF-5.[14]

Volume−pressure curves that directly reflect the mechanical properties of an individual desolvated ZIF-8 microcrystal (Figure S12). The ZIF-8 framework has ∼25% solvent-accessible free volume based on calculations using the PLATON software package.[3a,15] As shown in Figure S12, there are four steps involved in a single cycle: (1) the ZIF-8 microcrystal is compressed over the pressure range of 0−1.6 GPa with continuous volumetric reduction of 30% (0.48 μm^3 to 0.34 μm^3); (2) ZIF-8 resists further compression and maintains its volume as pressure is increased to ∼3 GPa; (3) the ZIF-8 microcrystal is compressed further to a maximum of 3.9 GPa with a total volume reduction of 58% (final volume 0.2 μm^3); and (4) upon release of pressure, the ZIF-8 microcrystal partially recovers to 69% of its original volume (i.e., 0.33 μm^3).

The distinct stepwise changes in volume shrinkage suggest the onset of amorphization at a pressure of ∼3 GPa, significantly higher than for the amorphization of bulk powder (∼1.1 GPa, Figure S4). The lowering of the onset of amorphization may be due to local focusing of pressure from microcrystal−microcrystal interactions (e.g., a sharp point of one microcrystal being pushed into the flat surface of its neighbor), which can play an important role in the amorphization of bulk samples. As the amorphization begins to occur in the individual microcrystal (350−450 nm displacement), the loading modulus (Figure 4) increases; this increase is due to the increasing density of the material as compression of internal void volume occurs within the ZIF-8 structure.

ZIF-8 is an anisotropic material, and the mechanical properties are fully dependent on the orientation of applied forces.[4d,12] For this reason, we compared the mechanical behavior of desolvated 1.2 μm ZIF-8 microcrystals compressed against the square facet (i.e., the (100) facet; Figures S7, S8, and S13) versus compression against the hexagonal facet (−101). Compression against the square projection is slightly easier with a constant loading Young's modulus (E_{load} = 3.2 ± 0.3 GPa over the displacement range of 100−240 nm, equivalently the force range of 200−850 μN) versus compression against the hexagonal face (E_{load} = 4.6 ± 0.2 GPa, Figure S14). The E_{unload} values are similar (45 ± 6 GPa for the square projection vs 41 ± 4 GPa for the hexagonal projection), suggesting that a similar dense amorphous phase was reached after maximum compression in both cases. The volume shrinkage of ZIF-8 microcrystals at a compression pressure of 2.6 GPa was ∼50% for the square face vs ∼70% for the hexagonal face; upon release of pressure, the square face recovers to 80% of its original volume vs 65% for the hexagonal face (Figure S15). Finally, compression against the square (100) facet began amorphization of the crystal at a lower pressure (∼2 GPa), compared to compression against the hexagonal (−101) facet (∼3 GPa; see Figure S15). All of these data are consistent with greater ease of compression against the square (100) facet compared to the hexagonal (−101) facet.

Size can also have an important influence on the mechanical properties of micro- and nano- structured materials. We compare compression against hexagonal facets of individual 550 nm desolvated ZIF-8 nanocrystals (Figure S13) vs 1.2 μm ZIF-8 microcrystals with same hexagonal projection: E_{load} for 550 nm ZIF-8 nanocrystals (3.9 ± 0.5 GPa) is similar to E_{load} for 1.2 μm microcystals (4.6 ± 0.2 GPa; Figure S16) over the compression range of 100−360 nm (equivalent to the force range of 250−4300 μN). Upon unloading, the nanocrystals have less elasticity than the microcrystals: E_{unload} at maximum compression (Figures S9 and S13) for 550 nm nanocrystals (75 ± 9 GPa) is much larger than that for microcrystals (41 ± 4 GPa). One thus concludes that the smaller crystals are more easily compressed and also are less elastic upon unloading.

DOI: 10.1021/ja5113436
J. Am. Chem. Soc. 2015, 137, 1750−1753

Two prior methods have been published for mechanical characterization of MOFs: mercury porosimetry (the intrusion of mercury at high pressure[16]) and diamond anvil cell compression (DAC, to observe the behavior of a single crystal or crystalline powder[17]). DAC can be used with or without a pressure-transmitting medium (PTM). For instance, Moggach et al. reported that ZIF-8 single crystals have a reversible phase transition in DAC with a pressure range between 0 and 1.5 GPa through twisting the conformation of the 2-MeIm linkers to more accessible 6-ring pores. Methanol molecules used as a PTM are squeezed into the internal voids during pressurization to 1.47 GPa and re-released during releasing pressure.[4c] Chapman et al. reported that crystalline ZIF-8 powder exhibited an *irreversible* structural transition and amorphization in DAC either with a nonpenetrating fluid or without any PTM under 0.34 GPa pressure.[4a] Hu et al. continued to compress ZIF-8 to 1.6 GPa in DAC without a PTM followed by decompression and found that the pressure effect was *reversible*; further compression to 39 GPa resulted in an *irreversible* structural transition to a disordered or amorphous phase.[4b] DAC observations do not directly reveal mechanical behavior of single ZIF-8 crystals because of the existence of a strong host−guest relationship with the PTM or of the existence of microcrystal−microcrystal interactions without a PTM. In our *in situ* TEM compression tests, the mechanical behavior of single ZIF-8 crystals could be observed without the complications of other intercrystal or crystal−matrix interactions.

In summary, we directly observed the dynamic deformation process of individual desolvated ZIF-8 crystals under compression. From calculated single-crystal volume changes as a function of pressure, we observed the structure and mechanical behavior of individual ZIF-8 crystals as functions of crystal orientation and size, offering a new way to study the mechanical properties of porous materials. The presence of solvates within the pores of the ZIF-8 has a dramatic effect on the mechanical properties of the single crystals. Methanol-solvated ZIF-8 microcrystals are much less deformable than the desolvated microcrystals and shatter completely at very low applied force. Thus, the presence of solvate filling the pores of ZIF-8 makes the microcrystals extremely rigid, with near total loss of plasticity, relative to desolvated crystals.

■ ASSOCIATED CONTENT

Supporting Information

Experimental details and instrumentations; PXRD, SEM, TEM, and X-ray absorption spectra; load−displacement, Young's modulus−displacement, and volume−pressure curves of ZIF-8 crystals (PDF); and TEM videos for desolvated 1.2 μm ZIF-8 microcrystals, hexagonal projection (file si_003.mpg), solvated 1.2 μm ZIF-8 microcrystals (file si_002.mpg), desolvated 1.2 μm ZIF-8 microcrystals, square projection (file si_004.mpg), and desolvated 500 nm ZIF-8 nanocrystals (file si_005.mpg). This material is available free of charge via the Internet at http://pubs.acs.org.

■ AUTHOR INFORMATION

Corresponding Author

*ksuslick@illinois.edu

Notes

The authors declare no competing financial interest.

■ ACKNOWLEDGMENTS

We acknowledge grants from the U.S. Navy (MURI N000141210828, K.S.S.), NSF (DMR 1206355, K.S.S.), U.S. DOE-BES (DEFG02-05ER46217, S.D.), UIUC Frederick Seitz Materials Research Laboratory Central Facilities, the Advanced Photon Source supported by the U.S. DOE-BES (DE-AC02-06CH11357), and MRCAT supported by DOE and MRCAT members.

■ REFERENCES

(1) Furukawa, H.; Cordova, K. E.; O'Keeffe, M.; Yaghi, O. M. *Science* **2013**, *341*, 1230444.

(2) (a) Farha, O. K.; Eryazici, I.; Jeong, N. C.; Hauser, B. G.; Wilmer, C. E.; Sarjeant, A. A.; Snurr, R. Q.; Nguyen, S. T.; Yazaydın, A. O.; Hupp, J. T. *J. Am. Chem. Soc.* **2012**, *134*, 15016. (b) Deng, H.; Grunder, S.; Cordova, K. E.; Valente, C.; Furukawa, H.; Hmadeh, M.; Gándara, F.; Whalley, A. C.; Liu, Z.; Asahina, S. *Science* **2012**, *336*, 1018.

(3) (a) Fairen-Jimenez, D.; Moggach, S.; Wharmby, M.; Wright, P.; Parsons, S.; Duren, T. *J. Am. Chem. Soc.* **2011**, *133*, 8900. (b) Hu, Y.; Liu, Z.; Xu, J.; Huang, Y.; Song, Y. *J. Am. Chem. Soc.* **2013**, *135*, 9287. (c) Chapman, K. W.; Sava, D. F.; Halder, G. J.; Chupas, P. J.; Nenoff, T. M. *J. Am. Chem. Soc.* **2011**, *133*, 18583.

(4) (a) Chapman, K. W.; Halder, G. J.; Chupas, P. J. *J. Am. Chem. Soc.* **2009**, *131*, 17546. (b) Hu, Y.; Kazemian, H.; Rohani, S.; Huang, Y.; Song, Y. *Chem. Commun.* **2011**, *47*, 12694. (c) Moggach, S. A.; Bennett, T. D.; Cheetham, A. K. *Angew. Chem., Int. Ed.* **2009**, *48*, 7087. (d) Tan, J.-C.; Civalleri, B.; Lin, C.-C.; Valenzano, L.; Galvelis, R.; Chen, P.-F.; Bennett, T. D.; Mellot-Draznieks, C.; Zicovich-Wilson, C. M.; Cheetham, A. K. *Phys. Rev. Lett.* **2012**, *108*, 095502.

(5) (a) Park, K. S.; Ni, Z.; Cote, A. P.; Choi, J. Y.; Huang, R.; Uribe-Romo, F. J.; Chae, H. K.; O'Keeffe, M.; Yaghi, O. M. *Proc. Natl. Acad. Sci. U.S.A.* **2006**, *103*, 10186. (b) Li, Z.; Zeng, H. C. *J. Am. Chem. Soc.* **2014**, *136*, 5631.

(6) Shimida, M. In *Current Japanese Materials Research*; Senoo, M., Suito, K., Kobayashi, T., Kubota, H., Eds.; Elsevier Science: Amsterdam, 1995; Vol. *15*, p 131.

(7) (a) Cravillon, J.; Münzer, S.; Lohmeier, S.-J.; Feldhoff, A.; Huber, K.; Wiebcke, M. *Chem. Mater.* **2009**, *21*, 1410. (b) Cravillon, J.; Nayuk, R.; Springer, S.; Feldhoff, A.; Huber, K.; Wiebcke, M. *Chem. Mater.* **2011**, *23*, 2130.

(8) (a) Qian, J.; Sun, F.; Qin, L. *Mater. Lett.* **2012**, *82*, 220. (b) Kida, K.; Fujita, K.; Shimada, T.; Tanaka, S.; Miyake, Y. *Dalton Trans.* **2013**, *42*, 11128.

(9) Drisdell, W. S.; Poloni, R.; McDonald, T. M.; Long, J. R.; Smit, B.; Neaton, J. B.; Prendergast, D.; Kortright, J. B. *J. Am. Chem. Soc.* **2013**, *135*, 18183.

(10) Tan, J. C.; Cheetham, A. K. *Chem. Soc. Rev.* **2011**, *40*, 1059.

(11) (a) Ortiz, A. U.; Boutin, A.; Fuchs, A. H.; Coudert, F. X. *J. Phys. Chem. Lett.* **2013**, *4*, 1861. (b) Zhang, L.; Hu, Z.; Jiang, J. *J. Am. Chem. Soc.* **2013**, *135*, 3722.

(12) Tan, J. C.; Bennett, T. D.; Cheetham, A. K. *Proc. Natl. Acad. Sci. U.S.A.* **2010**, *107*, 9938.

(13) Eslava, S.; Zhang, L.; Esconjauregui, S.; Yang, J.; Vanstreels, K.; Baklanov, M. R.; Saiz, E. *Chem. Mater.* **2013**, *25*, 27.

(14) Bahr, D.; Reid, J.; Mook, W.; Bauer, C.; Stumpf, R.; Skulan, A.; Moody, N.; Simmons, B.; Shindel, M.; Allendorf, M. *Phys. Rev. B* **2007**, *76*, 184106.

(15) Spek, A. *J. Appl. Crystallogr.* **2003**, *36*, 7.

(16) (a) Beurroies, I.; Boulhout, M.; Llewellyn, P. L.; Kuchta, B.; Férey, G.; Serre, C.; Denoyel, R. *Angew. Chem., Int. Ed.* **2010**, *49*, 7526. (b) Neimark, A. V.; Coudert, F. X.; Triguero, C.; Boutin, A.; Fuchs, A. H.; Beurroies, I.; Denoyel, R. *Langmuir* **2011**, *27*, 4734.

(17) (a) Graham, A. J.; Tan, J.-C.; Allan, D. R.; Moggach, S. A. *Chem. Commun.* **2012**, *48*, 1535. (b) Lü, X.; Hu, Q.; Yang, W.; Bai, L.; Sheng, H.; Wang, L.; Huang, F.; Wen, J.; Miller, D.; Zhao, Y. *J. Am. Chem. Soc.* **2013**, *135*, 13947.

DOI: 10.1021/ja5113436
J. Am. Chem. Soc. 2015, 137, 1750−1753